

Available online at www.sciencedirect.com

SCIENCE @ DIRECT®

Applied Surface Science xxx (2005) xxx–xxx

applied
surface sciencewww.elsevier.com/locate/apsusc

Conductance fluctuation and degeneracy in nanocontact between a conductive AFM tip and a granular surface under small-load conditions

Deng-Zhu Guo^{*}, Shi-Min Hou, Geng-Min Zhang, Zeng-Quan Xue*Department of Electronics, Peking University, Beijing 100871, China*

Received 11 April 2005; accepted 29 July 2005

Abstract

Conductive-tip atomic force microscope (c-AFM) has been extensively used in measuring electrical properties of surface nanostructures, but the electrical conduction in c-AFM tip–sample contacts in nanometer scale is not well understood. In the present work, we experimentally investigated the electrical properties of the nanocontact between a W_2C -coated c-AFM tip and granular gold film under small-load (~ 5 nN) at ambient air conditions. We found that under a constant bias voltage (10 V), the electrical current passing through the tip–sample junction at fixed location of sample surface dramatically fluctuated and degenerated. By quantitatively estimating the mechanical and electrical aspects of the nanocontact, we explained the observed phenomena as mechanical instabilities, electron tunneling transport and atomic rearrangements at the contact junction. We think that our results are important for the realistic application of c-AFM in nanoelectronic measurement.

© 2005 Elsevier B.V. All rights reserved.

PACS: 07.79.Lh, 73.40.Cg, 72.10.Fk

Keywords: Atomic force microscope (AFM); Conductive-tip; Nanocontact; Conductance fluctuation and degeneracy

1. Introduction

Atomic force microscope (AFM) has been a powerful technique in nanotechnological applications such as topographical imaging, nanoobject manipulation, nanolithography and physical (e.g., mechanical,

thermal, magnetic and electrical) property measurements. By using a conductive-tip AFM (c-AFM), one can simultaneously obtain topographical and electrical properties of nanostructured surfaces, even build a nanoelectronic device prototype with a c-AFM tip as the connecting electrode [1–6]. Naturally, good tip–sample electrical contact, namely, small and stable contact resistance, is highly expected for these applications. However, at the present stage, the electrical transport in c-AFM tip–sample contact

^{*} Corresponding author. Tel.: +86 10 62762442;
fax: +86 10 62762442.

E-mail address: guodz@pku.edu.cn (D.-Z. Guo).

has not been explicitly understood, especially at small contact load conditions. Bietsch et al. [7] investigated the nanocontacts between a Pt-coated AFM tip and gold film and found that the conductance is stable only under large contact force (500–600 nN) and large contact width (~ 20 nm) conditions, but unstable under small-load situation. Houz e et al. [8] reported that the contact resistances are highly dispersed (10^2 – 10^{10} Ω) by scanning a W-coated c-AFM tip on W film. But they explained the resistance discrepancy only from the various oxidation states of the surface grains, instead of the inherent instabilities of this type of nanocontacts. In fact, the resistance instabilities, namely conductance fluctuation, in nanocontacts in scanning tunneling microscopy (STM) [9], in mechanically controllable break junctions (MCBJ) [10] and in metal nanobridges [11,12], have already been observed. These facts implied that the electrical contact in c-AFM tip–sample system would not be so good as common expectation in some realistic applications, in which due to the high imaging resolution and/or nondestructive requirements, the contact force applied between c-AFM tip and sample is often as small as several nN and the contact region a few nm. For instance, for building carbon nanotube (CNT) based devices with AFM tips as electrodes [3–6], the tip–CNT contact force must be small enough, because large contact force would induce mechanical deformation of CNTs and change their electrical properties [13]. Another example is the recently increasing interests in measuring the electrical conductance of organic molecule with c-AFM tip as the contact electrode, in which the contact load should also be in nN order [14,15]. Meanwhile, sputtered/evaporated gold films are usually used as conductive substrates in most of c-AFM electrical measurements. Therefore, it is of significance to do researches directly on small-load c-AFM nanocontact with real granular gold films. This is our original motivation of this work.

In the present paper, we experimentally investigated the electrical nanocontacts between W_2C -coated AFM tips and granular gold films under small-load in the ambient air environment and found that the resistance instability in such a system is very strong. In addition to conductance fluctuation, we have also observed the phenomena of conductance degeneracy in this system. Subsequently, we proposed a ball-particle contact model to demonstrate the mechanical instabilities and used Simmons' tunneling theory to

interpret the large contact resistance. Based on the quantitative estimation of the mechanical and electrical aspects of the nanocontact, these observed phenomena were explained as the mechanical variation of the contact junction, the change of the tunneling barrier and the atomic rearrangement in the contact region. Our results remind that one should be cautious in nanoelectronic measurements with conductive AFM tips as contacting electrodes.

2. Experiment

2.1. Sample preparation

The gold films were prepared on silicon wafer by using a radio frequency magnetron sputtering system. Before deposition, the substrates were ultrasonically cleaned in acetone and ethanol for 5 min, respectively and heated to ~ 180 $^\circ\text{C}$ in 5×10^{-4} Pa for 30 min in order to remove the water vapor adsorbed on the surface. Then, argon gas was input into the chamber at 30 sccm till total pressure reached to ~ 0.8 Pa. After cleaning the gold target (purity 99.99%) surface by pre-sputtering, ~ 2 μm thick gold films were deposited onto the wafer substrate at a rate of ~ 2 nm/s. At last, Ar^+ ion beam with energy of 500 eV and density of 0.3–0.5 mA/ cm^2 was used to bombard the deposited films for 2 min in order to improve the surface structures.

2.2. Experimental setup

A commercial scanning probe microscope (Solver NT-MDT-P47, made in Russia) worked in contact-AFM mode under ambient air was used. This apparatus has electrical measurement accessories and allows measuring electrical properties of samples, such as current–voltage (I – V), current–time (I – t) and localized capacitance, with a conductive probe. Piezoelectric tubes and laser deflection–split photodiode assemblies are used as the micro-movement controlling system. A cone tip dwelling on one end of a rectangular silicon cantilever was used as the probe. The naked tip with curvature radius of less than 35 nm was coated with ~ 25 nm W_2C films (according to the tip manufacturer). The vertical movement Δz of the tip, equaling to the upward deflection of the cantilever end induced by the tip–sample interaction, was used as

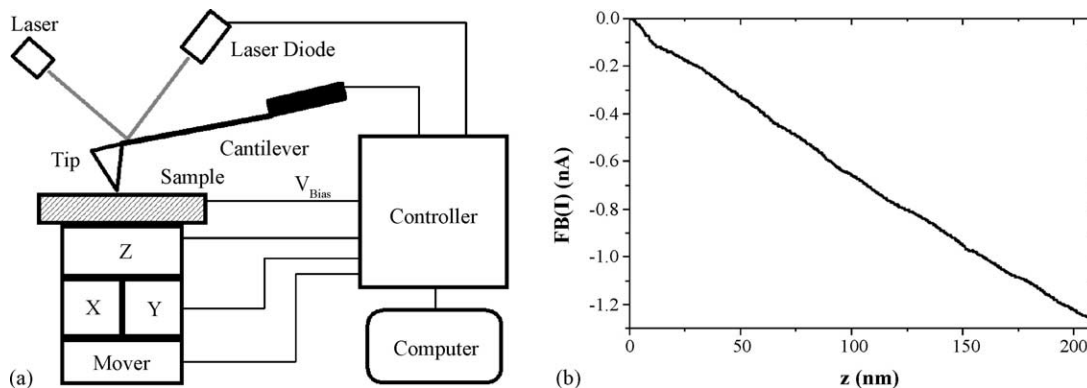


Fig. 1. (a) Schematic experimental setup of conductive-tip AFM. (b) $FB(I)$ - z curves measured under feedback gain = 6, showing that the feedback sensitivity of the z -piezoelectric tube is ~ 160 nm/nA. From the feedback input 1 nA and the force constant 0.03 N/m of the cantilever, the contact load is estimated as ~ 5 nN.

the feedback signal through the laser reflection system. An adjustable DC voltage can be biased between the tip and sample and the current passing through the tip-sample junction can be recorded versus bias voltage or time. The experimental setup is schematically shown in Fig. 1(a).

2.3. Experimental methods

After approaching the tip and making it “touch” the sample surface, firstly we measured the $FB(I)$ - Δz curves (Fig. 1(b)) under feedback gain = 6, here $FB(I)$ is the feedback input current and Δz the vertical movement of piezoelectric tube, equaling to the upward deflection of the cantilever end when tip-sample contact is established. We found that the z -piezoelectric tube extends ~ 160 nm by inputting 1 nA feedback current under feedback gain = 6. From the relative Setpoint of 1 nA (Setpoint equals to -1 and 0 nA, respectively, before and after the contact established) and the cantilever force constant of ~ 0.03 N/m, we knew that the contact load (repulsive force between the tip and the sample) was ~ 5 nN, much smaller than 500–600 nN used by Bietsch et al. [7] to obtain stable contacts. Subsequently, a 10 V DC constant voltage (or scanning voltage) was negatively biased to the sample and the current evolving with time (or current-voltage) was recorded with a data-acquisition frequency of 100 Hz. Topographical images were also obtained at the same surface location before and after the conductance measurements for comparison.

Additionally, for verifying the experimental phenomena, some comparative experiments were also conducted under large contact force (~ 150 nN) conditions by using a similar cantilever with force constant of ~ 0.3 N/m and the same experiments were repeated with a different AFM apparatus (Digital Nanoscope III(a)) and different kinds of conductive-tips (Au-coated and TiN-coated tips).

3. Results

3.1. Preliminary surface morphology of the gold film

After contacting the tip with the sample at ~ 5 nN contact load, an image of the gold film with a good resolution was scanned in contacting AFM mode (Fig. 2), showing that the surface of the sample consists of nanoparticles with diameters of ~ 100 nm, with a surface root mean square (rms) roughness of ~ 5 nm. This also approves that the mechanical contact has been well established between the tip and the sample surface, although the contact force is very small.

3.2. Nonrepeatability of I - V curves on the same surface location

One of the most widely used techniques of c-AFM is to measure the electrical properties of a sample by

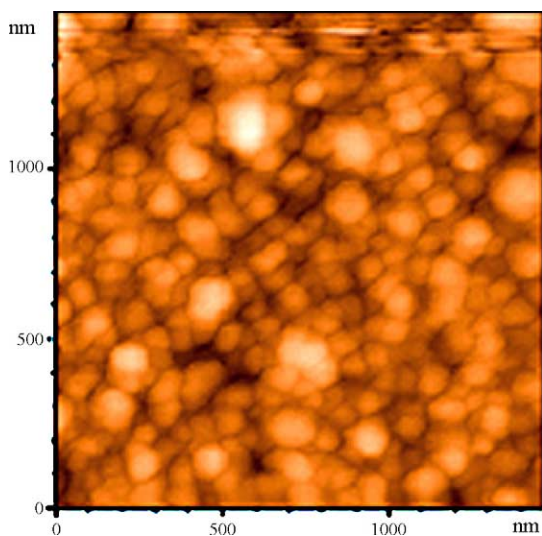


Fig. 2. Surface morphological image of the gold film obtained by using contact AFM under ~ 5 nN contact load, showing a granular nature.

recording I - V curves of the tip-sample system. We usually found that under the ambient air conditions, the repeatability of I - V measurement for most kinds of samples is very poor. Fig. 3 shows three typical I - V curves obtained at the same surface location of the gold film with W_2C -coated c-AFM tip under ~ 5 nN load condition. The curves A, B and C are very different from each other: in curve A, there is no detectable current within all the ± 10 V voltage range; in curve B, current appears only above positive voltage $+8$ V; and in curve C, except for a dead bias region

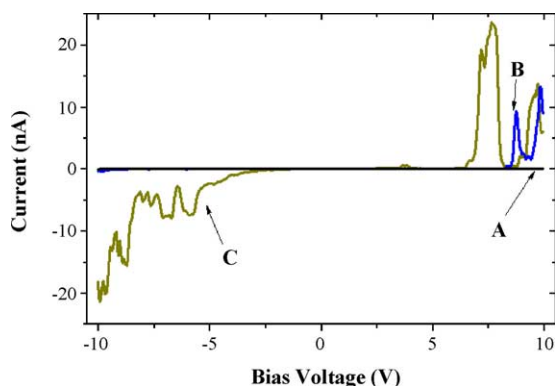


Fig. 3. Nonrepeatability of I - V curves measured in the same location of the sample surface.

(-2.5 to $+6.5$ V), current appears asymmetrically at both positive and negative bias end. Additionally, it is strange to note the negative resistance peaks (current decreases with voltage increasing) in curves B and C. Obviously, these I - V curves are not usable in judging the sample electrical properties, but imply that the tip-sample contact system might be electrically unreliable.

3.3. Conductance fluctuation and degeneracy phenomena

In order to investigate the reliability of the tip-sample electrical contact, we applied 10 V bias voltage between the tip and sample (sample negative) at a fixed surface location and recorded the current-time curves. Unsurprisingly, we found that the current is not stable under the constant bias voltage, instead, behaves like random pulses, as shown in Fig. 4. During the first few minutes, the pulse density increases gradually and then it begins to decrease. The typical pulse behavior after biased 1, 15, 30 and 40 min are respectively displayed in Fig. 4(a)–(d), showing that the current pulses have the tendency to change from dense to sparse with time and their amplitude also gradually decrease. The apparent contact resistance, estimated by V/I , is changed between 400 M Ω and

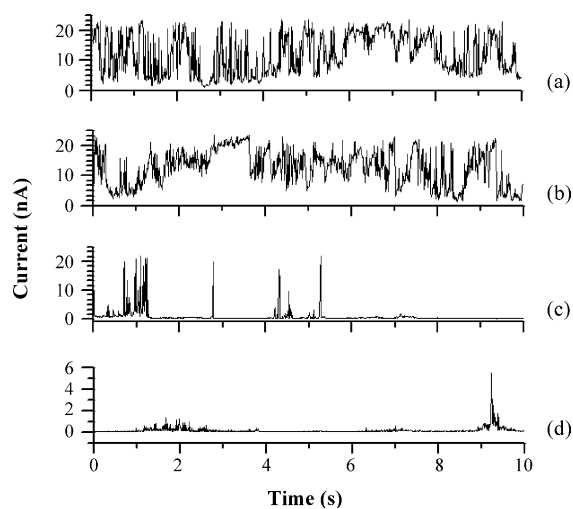


Fig. 4. Current fluctuation and degeneracy behaviors in the nanocontact under constant ~ 5 nN contact load and 10 V bias voltage. The I - t curves after biased 1 min (a), 15 min (b), 30 min (c) and 40 min (d) are shown, respectively.

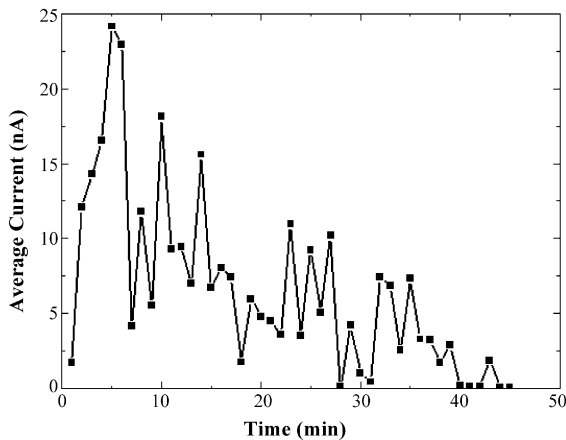


Fig. 5. The degenerative behavior of the average current, noting it becomes completely undetectable after biased 45 min.

10 G Ω for most time. After 45 min, the current attenuated to an undetectable value and no current recovered afterwards. The whole process is averagely shown in Fig. 5, which displays that the average current, obtained by arithmetically averaging the current data within every minute, degenerates in oscillation with time.

When current ultimately became unmeasurable, we removed the 10 V bias voltage and waited statically for 10–30 min and then applied it again, and found that the pulse-current phenomena are gradually reproducible in partial.

3.4. Surface morphologies after the $I-t$ measurement

After the $I-t$ measurement till the current degenerated to an unmeasurable value, a series of topographical images were scanned at different time for comparison. At the beginning, a very blurred image compared with Fig. 2 at the same surface location was obtained, showing a decreased image resolution (Fig. 6). Statically waiting for 10, 20 and 30 min and scanning images at the same place again and again, we found that the image resolution gradually became better and better and at last nearly recovered to the original one as Fig. 2.

3.5. Comparative experiment results

In order to exclude the possible dependence of the observed phenomena on the apparatus, the tip

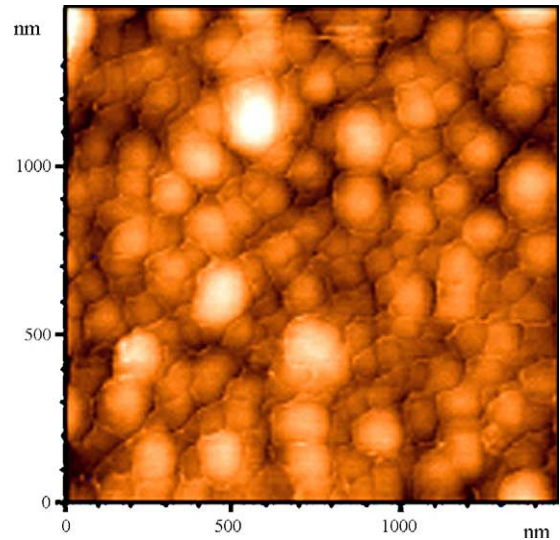


Fig. 6. AFM image of the gold surface morphology obtained after $I-t$ measurements, looking much more blurred in comparison with the preliminary image of Fig. 2 at the same surface location.

coatings, the circuits and the environmental vibration, we did some comparative experiments. The leak current of the circuit was checked as 10–20 pA, three orders less than the amplitudes of the pulses. The fineness of vibration-isolation system of the apparatus was attested by easily obtaining atomic resolution of highly oriented pyrolytic graphite (HOPG) in STM mode. Moreover, using Au-coated and TiN-coated AFM tips to contact with evaporated or sputtered gold films and doing the same experiments in an apparatus of Digital Nanoscope III(a) with Keithley electrical

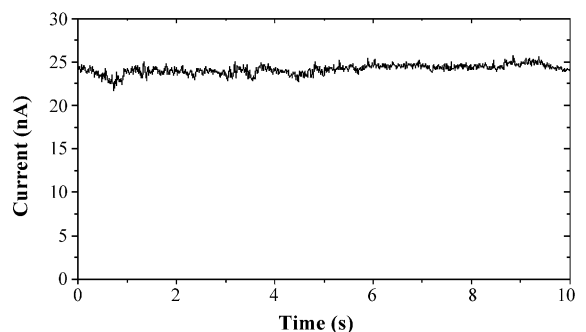


Fig. 7. A comparative $I-t$ measurement under a large (~ 150 nN) contact load condition.

measurement accessories, the similar phenomena were also observed.

At last, we did an experiment with a large contact load of about 150 nN by using a similar cantilever with force constant about ~ 0.3 N/m under Setpoint 3 nA and found that the electrical contact was well improved. The typical $I-t$ curve was shown in Fig. 7, in which despite the current also fluctuates, it became much more smaller. The conductance degeneracy phenomena have not been observed during a half-hour measurement period. Noteworthy is that the apparent contact resistance is also very high, even under the large contact load.

4. Discussion

4.1. Mechanical contact between an AFM tip and real granular surfaces

In order to interpret the observed phenomena, we firstly consider the mechanical aspects of the nanocontact. It has been shown that the continuum contact mechanics can be used in nanocontact estimates [7,8,16]. We assume that the Hertz elastic contact theory [17] is pertinent to our small-load conditions. Unlike the ball-plane contact models used in the previous studies [7,8], now we consider an AFM tip contact with a real granular surface. For simplification, the surface particles are seen as spherical shape with the same radius R_s and the AFM tip is seen as a smaller ball with a radius R_t . As schematically shown in Fig. 8, the general contact mode is in case (A), in which one can see the force analysis about the tip, mainly including normal constant load N from the cantilever deflection and

the real contact force F from the surface particle. Since the force F has an angle θ relative to the normal direction, it can be decomposed to two forces F_1 and F_2 and the former is balanced with N . In order to realize equilibrium, another force F'_2 should be provided by the cantilever torsion to balance the force F_2 . Obviously, the real contact force F and the lateral component F_2 are

$$F = \frac{N}{\cos \theta} \quad (1a)$$

$$F_2 = N \tan \theta \quad (1b)$$

That means the real contact force F could be larger than the normal load N and the lateral force F_2 could be comparable with N due to the arbitrary θ angle.

If θ is large enough, namely $\theta = \theta_{\max}$, the tip would simultaneously contact with two surface particles (two-dimensional assumption), as shown in Fig. 8 case (B), each contact force is $F = N/2 \cos \theta_{\max}$. On the other hand, if $\theta = 0$, it leads to contact force $F = N$ (Fig. 8 case (C)), which is one specific case of status (A). Under these two special situations, the lateral balance will be naturally realized without the cantilever torsion.

Now we estimate the real contact width. From Hertz contact theory about two-ball contact, the tip-particle contact radius can be calculated as

$$r = \left(\frac{3FR^*}{4E^*} \right)^{1/3} \quad (2)$$

where $1/R = 1/R_s + 1/R_t$, $1/E^* = (1 - \nu_s^2)/E_s + (1 - \nu_t^2)/E_t$. Here F denotes the contact force, R_s and R_t are the particle and tip radius and ν_s , ν_t , E_s and E_t , respectively, the Poisson ratios and Young's moduli of the gold sample and W_2C -coated tip. Taking $R_s = 100$ nm, $R_t = 60$ nm, $\nu_s = 0.42$, $E_s = 77.5$ GPa, $\nu_t = 0.28$ and $E_t = 350$ GPa and thinking about the case (C), in which $F = N = 5$ nN, we get $r_c \approx 1.23$ nm. That means, in case (C), the contact width is $2r_c \approx 2.5$ nm and the contact area is $S_C \approx 4.8$ nm². Noteworthy is that the contact radius is of quantum size, much smaller than $r > 10$ nm in Ref. [7]. We also note that under case (B), since $\cos \theta_{\max} = \sqrt{2R_s R_t} / (R_s + R_t) \approx 0.7086$, the contact force at each contact point is $F = 3.53$ nN and contact radius $r_B = 1.12$ nm, a little smaller than r_C , but the total contact area is $S_B = 2\pi r_B^2 \approx 7.88$ nm², much larger than S_C .

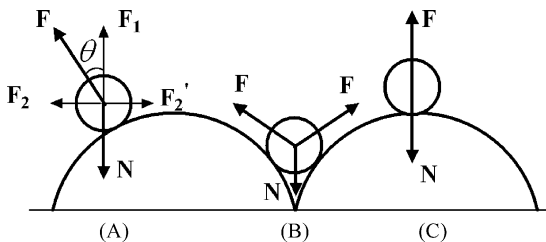


Fig. 8. A schematic model of an AFM tip (small ball) contact with a granular surface.

Similarly, it is easy to write out the contact radius $r_A = r_C / (\cos \theta)^{1/3}$ for case (A), in which r_A slightly varies with the angle θ . Similar estimates could be carried out about the maximum contact stress and the indentation depth, which also varies in the three cases.

The above consideration suggests that for the static contact between an AFM tip and a granular surface, the contact parameters such as contact force, contact area, stress and indentation depth, are markedly variable even under a constant load condition. Additionally, some lateral forces are also involved in the static-like contact, which would induce lateral instabilities. Keeping this point in mind, one can image that under small-load conditions, since both the normal and lateral balancing forces are very small, the general contact equilibrium would be unstable and easily intervened by the outer influences such as the capillary force coming from the water adsorption, the electrostatic force and the creepage of the piezo-tube. Hence some relative micro-motions could occur between the tip and particles and induce changes of the contact status. Otherwise, if a large contact load is applied, the normal and lateral balancing forces are also large and not easily effected by outer factors. Moreover, the contact status is more likely reach to the case (B) through a large torsion of the cantilever. Therefore, the mechanical contact under large contact load conditions is more stable.

4.2. Electrical transport and apparent contact resistance

Secondly, we consider the electron transport modes in the tip–sample contact. If a real electrical contact is established between the AFM tip and particle surface, i.e., no insulating layer exists between the two conductors, the electrons transport through the contact junction possibly by scattering and/or ballistic modes. The size-dependent contact resistance of each contact point comes from the constriction resistance R_C , which is the solution of a Laplace equation with appropriate boundary conditions [18]

$$R_C = \frac{4(\rho_1 + \rho_2)\lambda}{9\pi r^2} + \frac{\rho_1 + \rho_2}{2\pi r} \int_0^\infty \exp(-x\lambda/r) \frac{\sin(\pi x)}{\pi x} dx \quad (3)$$

where ρ_1 and ρ_2 are the specific resistivities of the materials in contact, respectively, λ is the average electron free path, i.e., $\lambda = (\lambda_1 + \lambda_2)$ and r is the contact radius. Specifically, if $r < \lambda$, R_C is dominated by Sharvin's ballistic mechanism [19] and the equation reduces to

$$R_S = \frac{\lambda(\rho_1 + \rho_2)}{2\pi r^2} \quad (4)$$

Alternatively, if $r < \lambda$, the scattering mode is dominant and the contact resistance is reduced to the Maxwell formula [20]

$$R_M = \frac{\rho_1 + \rho_2}{4r} \quad (5)$$

In our case, the condition $r < \lambda$ is well satisfied, since for most conductors, $\lambda = 10\text{--}100$ nm. So Eq. (4) seems to be appropriate for estimating the contact resistance. Taking appropriate values into these equations, namely, $\rho_1 = 2.2 \mu\Omega \text{ cm}$, $\rho_2 \sim 2 \text{ m}\Omega \text{ cm}$, $\lambda = 10$ nm and $\pi r^2 \sim 5 \text{ nm}^2$, we found that the calculated resistance ($\sim 20 \text{ K}\Omega$) is much more lower in several orders than the experimental results.

So, we assume that a very thin ($\sim 5 \text{ \AA}$) insulating layer (monolayer) exists in the contact junction. Because the experiments were carried out in the ambient air environment, the physical and/or chemical adsorptions are inevitable. Meanwhile, because of the small contact force, the contaminant layer cannot be penetrated completely. Hence, the assumption of atomic insulating layers existing in surfaces might be reasonable. In this situation, the electrons transport through the contact junction in tunneling mode. The tunneling current density J (in A/cm^2) is given by Simmons for arbitrary shaped potential barriers and voltages [21]

$$J \approx \frac{6.2 \times 10^{10}}{\Delta s^2 \{ \bar{\phi} \exp(-1.025\Delta s \cdot \bar{\phi}^{1/2}) - (\bar{\phi} + V) \exp[-1.025\Delta s \cdot (\bar{\phi} + V)^{1/2}] \}} \quad (6)$$

where Δs (in \AA) and $\bar{\phi}$ (in V) are the width and average height of the potential barrier, respectively and V the bias voltage. The apparent contact resistance is simply given by $R_T = V/\pi r^2 J$. Taking $\Delta s \sim 5 \text{ \AA}$, $\bar{\phi} \sim 4 \text{ V}$ and $V = 10 \text{ V}$, we get $R_T = 440 \text{ M}\Omega$, which is reasonable compared to our experimental results, meaning that tunneling is the dominant transport mode in our case.

Alamarguyb et al. recently reported that when a monolayer exists on sample surfaces, the electrical contact between a c-AFM tip and sample would not be established synchronously with the mechanical contact [22]. Therefore, we deduce that the real electrical contact has not been established in our case, which could also be seen in the typical I - V curves (Fig. 3) due to the existence of the wide dead-bias region.

4.3. Mechanisms of the conductance fluctuation and degeneracy

Having known that there are possible mechanical instabilities in tip–particle contact and tunneling is the dominant transport mode in the contact junction, we now could comprehend the conductance fluctuation and degeneracy phenomena. Due to the relative micro-motion of the tip under small-load conditions, the contact junction is always in micro changing, so the real contact force, contact area, stress and indentation depth are not static, but in variation. That means the tunneling barrier parameters ($\Delta s, \bar{\phi}$) are changing. Noting that they appear in exponents in Eq. (6), the large extent of the conductance fluctuation is reasonable.

Additionally, some physical and chemical changes are also possible for the changes of the tunneling barrier parameters ($\Delta s, \bar{\phi}$). Firstly, because the liquidized water vapor bridges the tip–sample by sides, electrochemical reactions such as oxidation of the contact surfaces could occur, which tend to change the surface states permanently. Secondly, because of the quantum size of contact radius, the current density in the contact is very high ($\sim 10^5$ A/cm²), the electric field cross the two conductors is very strong ($\sim 2 \times 10^8$ V/cm) and the Joule heating power density is very large ($\sim 10^6$ W/cm²). These mean that the atoms and especially, the atomic defects, in the vicinity of contact junctions are in the states far from equilibriums. Electromigration of defects could occur under such extreme conditions because of their large electron scattering sections. The electromigration could induce changes of atomic arrangement in contact and induce defect concentration near the contact junction [9–12]. All these chemical and physical processes could randomly change the average barrier height $\bar{\phi}$ and barrier width Δs in Eq. (6) and result in the large conductance fluctuations. With time

evolution, the surface oxidation and the defect concentration near the contact becomes greater and greater and so the average current becomes less and less. When the process reaches to a critical value, the electrical current is completely undetectable at last. Removing the bias voltage for a few minutes, the concentrated defects near the contact will diffused back at least partially because of the gradient of the defect density. Then, applying the bias again, we found that the pulse current recovered.

The above explanations of the conductance instabilities are partially supported by the morphologic observations. Compared with the original image in Fig. 2, the image after the I - t measurement in Fig. 6 has a blurred resolution, evidencing that the surface structures of the gold film and/or the AFM tip have changed during the I - t measurements. After the I - t measurements, the images scanned in the same region in series show a tendency of gradual recovery to a better resolution as in Fig. 2, suggesting that the changed surface status could partially reversible.

From the above explanation, the nonrepeatability of the I - V measurements as shown in Fig. 3 are also easily understandable. Due to the instabilities of the contact junction, the separated I - V measurements would not be in the same contact status, variation of the tunneling barriers would induce different kinds of I - V curves. The asymmetry of the I - V curves about the negative and positive bias voltages also comes from the tunneling barrier difference of the tip and sample materials.

5. Conclusion

Small-load nanocontact between a c-AFM tip and a real granular Au surface is much more complex than most common expectations. Under several nN of the contact load, the real electrical contact could not be efficiently established between the two conductors due to various physical and chemical adsorptions on the tip and sample surfaces. So the electrons have to pass through the contact junction by tunneling mechanism. The mechanical instabilities, as well as some physical and chemical processes, could induce the variations of the tunneling barrier parameters, which exponentially influence the apparent contact resistance. That is the reason of the conductance fluctuation in the

nanocontact. The extreme physical and chemical conditions near the contact junction would also induce the atomic rearrangement in the contact junction and the defect concentration would be responsible for the conductance degeneracy. We think that our work is of importance for the realistic application of the c-AFM in the electrical measurements of nanostructured surfaces.

Acknowledgements

We are grateful to Prof. C. W. Wang for help in partial experiments, to Dr. J. Luo for enlightening discussion. We also acknowledge the financial support from the National Natural Science Foundation of China (Nos. 60231010 and 60471008).

References

- [1] X.D. Cui, A. Primak, X. Zate, J. Tomfohr, O.F. Sankey, A.L. Moore, T.A. Moore, D. Gust, G. Harris, S.M. Lindsay, *Science* 294 (2001) 571.
- [2] A. Bachtold, M.S. Fuhrer, S. Plyasunov, M. Forero, E.H. Anderson, A. Zettl, P.L. McEuen, *Phys. Rev. Lett.* 84 (2000) 6082.
- [3] P.J. de Pablo, M.T. Martnez, J. Colchero, J. Gomez-Herrero, W.K. Maser, A.M. de Benito, E. Munoz, A.M. Baro, *Mater. Sci. Eng. C* 15 (2001) 149.
- [4] T.W. Tomblor, C. Zhou, J. Kong, H. Dai, *Appl. Phys. Lett.* 76 (2000) 2412.
- [5] S.J. Tans, C. Dekker, *Nature (London)* 404 (2000) 834.
- [6] Y. Otsuka, Y. Naitoh, T. Matsumoto, T. Kawai, *Appl. Phys. Lett.* 82 (2003) 1449.
- [7] A. Bietsch, M.A. Schneider, M.E. Welland, B. Michel, *J. Vac. Sci. Technol. B* 18 (3) (2000) 1160.
- [8] F. Houz , R. Meyer, O. Schneegans, L. Boyer, *Appl. Phys. Lett.* 69 (1996) 1975.
- [9] N. Agra t, J.G. Rodrigo, S. Vieira, *Phys. Rev. B* 47 (1993) 12345.
- [10] C.J. Muller, J.M. van Ruitenbeek, L.J. de Jongh, *Phys. Rev. Lett.* 69 (1992) 140.
- [11] P.A.M. Holweg, J. Caro, A.H. Verbruggen, S. Radelaar, *Phys. Rev. B* 45 (1992) 9311.
- [12] K.S. Ralls, D.C. Ralph, R.A. Buhrban, *Phys. Rev. B* 40 (1989) 11561.
- [13] T.W. Tomblor, C. Zhou, L. Alexseyev, J. Kong, H. Dai, L. Liu, C.S. Jayanthi, M. Tang, S.Y. Wu, *Nature (London)* 405 (2000) 769.
- [14] S. Tanaka, L.T. Cai, H. Tabata, T. Kawai, *Jpn. J. Appl. Phys.* P1 42 (2003) 2818.
- [15] T. Ishida, W. Mizutani, T.T. Liang, H. Azebara, K. Miyake, S. Sasaki, H. Tokumoto, *Mol. Electron. III Ann. NY Acad. Sci.* 1006 (2003) 164.
- [16] G. Rubio, N. Agra t, S. Vieira, *Phys. Rev. Lett.* 76 (1996) 2302.
- [17] K.L. Johnson, *Contact Mechanics*, Cambridge University Press, Cambridge, 1985, p. 91.
- [18] L. Kogut, K. Komvopoulos, *J. Appl. Phys.* 94 (2003) 3153.
- [19] Y.V. Sharvin, *Sov. Phys. JETP* 21 (1965) 655.
- [20] R. Holm, *Electrical Contacts*, 4th ed., Springer, New York, 1967, pp. 9–16.
- [21] J.G. Simmons, *J. Appl. Phys.* 34 (1963) 1793.
- [22] D. Alamarguyb, O. Schneegans, S. No l, L. Boyer, *Appl. Surf. Sci.* 225 (2004) 309.